Structural Investigation of Vanadyl-Acetylacetonate-Containing Precursors of TiO_x-VO_x Mixed Oxides on SBA-15

S. Van Doorslaer,*,† Y. Segura,‡ and P. Cool‡

Laboratory for Spectroscopy in Biophysics and Catalysis, Departments of Physics, and Laboratory of Adsorption and Catalysis, Department of Chemistry, University of Antwerp, Universiteitsplein 1, B-2610 Wilrijk, Belgium

Received: July 29, 2004; In Final Form: October 7, 2004

TiO_x-VO_x mixed-oxide supported SBA-15 catalysts were prepared by the molecular designed dispersion method (MDD) using acetylacetonate complexes. Two different synthesis route depositions are presented to prepare these mixed-oxide catalysts in a very controlled way. Continuous wave and pulse EPR spectroscopy is employed to determine the location of the $VO(acac)_2$ complexes in the mixed-oxide precursors (before calcination) in comparison to other supports. It is shown that the different synthesis pathways lead to differences in the local structure of the VO^{2+} complexes and to a distinctive degree of spreading of the metals on the support surface. This is confirmed by additional characterizations of the final catalyst in terms of chemical composition and porosity. Depending on the way of preparation of the mixed oxides, the final catalysts present significant differences in pore structure, showing partially blocked or open mesopores. In the case of the mixed-oxide samples a higher dispersion of the metals is observed compared to the disposition of $VO(acac)_2$ on the pure SBA-15 support. Both hyperfine sublevel correlation (HYSCORE) and IR spectroscopy show that the $VO(acac)_2$ complex, in contrast to the $TiO(acac)_2$ complex, has a great tendency to increase its coordination sphere by coordinating water molecules, but that this tendency is highly reduced when $VO(acac)_2$ is present in a Ti environment.

Introduction

Many strategies have been described in the literature for the immobilization of redox-active species within an inorganic matrix for the catalytic applications, by means of incorporation of transition metals during synthesis,[1−3] or grafting directly by postsynthesis for example by impregnation.[4−6] Materials containing V and Ti are very suitable for a number of selective reduction−oxidation reactions. One of the most studied processes is the selective catalytic reduction (SCR) of NO_x. Commercially, SCR catalysts are mostly based on vanadia/titania and sometimes also tungsten oxides and/or molybdenum oxides. Various methods for their preparation have also been reported in the literature.[7,8] One of the more successful supports for vanadium in the selective oxidation reactions is TiO_2. In fact, in the oxide forms Ti interacts strongly with V, but its use as a support is limited by the fact that it possesses a low specific surface area and a low resistance to sintering. On the other hand, the interaction of V with silica is weaker but silica has the advantage of a high specific surface area, and a higher resistance to sintering.

The VO_x-TiO_x/SBA-15 catalysts presented in this study are synthesized following two different synthesis pathways by the molecular designed dispersion process (MDD),[9−12] where the metal acac complexes (acac = acetylacetonate) are reacted with the surface hydroxyls of the support material, and converted into the metal−oxide form after calcination. On one hand, the SBA-15 material is a new type of material, which has very interesting properties to act as a support in the MDD process. It presents high thermal and hydrothermal stabilities. Furthermore, these ordered hexagonal SBA-15 materials, are characterized by a narrow pore-size distribution, high pore volumes, thick pore walls, intrinsically combined micro- and mesopores, and high surface area exceeding 800 m^2/g. On the basis of these attractive properties, SBA-15 can be used in many applications such as catalytic support, adsorbent for heavy metals, and immobilization of enzymes. On the other hand, it has already been reported that the catalytic activity of a V-supported silica catalyst increases when coating the silica support with a monolayer of TiO_2.[13,14] Therefore, we are expecting that the VO_x-TiO_x/SBA-15 catalysts have advantages compared to conventionally prepared VO_x/SBA-15 or VO_x/TiO_2. The detailed results on the catalytic properties of these catalysts will be reported in a following paper.

This paper focuses on the investigation of the interactions between the V- and Ti-containing centers and/or the OH of water or the silica support with the emphasis on the use of EPR (electron paramagnetic resonance) spectroscopy. By means of continuous wave (CW) and pulse EPR spectroscopy the local environment of the VO^{2+} complexes in the noncalcined precursors of the TiO_x-VO_x/SBA-15 mixed-oxide catalysts is studied. In addition, comparative analyses of $VO(acac)_2$ complexes on different supports and in various solvents are performed in order to elucidate the results obtained for the catalyst precursors. The interpretations of the EPR data are also supported by IR studies. The EPR and IR findings on the precursors give insight into the structure of the final catalysts. Indeed, it is clear that the specific V−Ti−support interactions in the precursor will greatly influence the structure and size of the catalyst and, as a consequence, will have a large impact on the catalytic properties.

* Corresponding author. Telephone: 0032-3-8202461. Fax: 0032-3-8202470. E-mail: sabine.vandoorslaer@ua.ac.be.
† Department of Physics, University of Antwerp.
‡ Department of Chemistry, University of Antwerp.

10.1021/jp046611l CCC: $27.50
Published on Web 12/09/2004

TABLE 1: Overview of the Samples Used in This Work

sample numbering	sample description
1	$VO(acac)_2-TiO(acac)_2$−SBA-15
2	$VO(acac)_2-TiO_x$−SBA-15
3	$VO(acac)_2-TiO_x$
4a	$VO(acac)_2$−SBA-15 (dry)
4b	$VO(acac)_2$−SBA-15 (wet)
5	$VO(acac)_2$ in $TiO(acac)_2$ (0.1 in 99.9 wt %)
6	$VO(acac)_2$ in dry toluene (3 mM)
7	$VO(acac)_2$ in ethanol (3 mM)

Materials and Methods

Table 1 gives an overview of the samples under study and shows the numbering by which the samples will be indicated throughout this work.

Materials. *Synthesis of the Support*. SBA-15 was prepared by using 4 g of Pluronic P123 triblock copolymer surfactant ($EO_{20}-PO_{70}-EO_{20}$) dissolved in water/HCl 2 M solution. Subsequently, an amount of TEOS (tetraethyl orthosilicate) was added. The resulting mixture was stirred for 8 h at 45 °C and then aged for 15 h at 80 °C. The white product was filtered, washed and dried. The sample was subsequently calcined at 550 °C with a heating rate of 1 °C/min and an isothermal period of 6 h in air atmosphere. Commercially available titanium oxide (P25 from Degussa) was also used as support.

Metal Deposition. Sample **5** was synthesized by wet impregnation of 0.1 wt % $VO(acac)_2$ and 99.9 wt % $TiO(acac)_2$ in toluene. Samples **6** and **7** were prepared by dissolving $VO(acac)_2$ in dry toluene (3 mM) and in ethanol (3 mM), respectively. Single depositions of $VO(acac)_2$ on the ordered mesoporous material SBA-15 (**4a**, **4b**) and on the TiO_2 support (**3**) were done by the MDD method of the acetylacetonate complex, as well as the mixed-oxide deposition of the two metals on the SBA-15 support (**1**, **2**). Deposition of the metal acetylacetonate complex ($TiO(acac)_2$ and/or $VO(acac)_2$) onto the SBA-15 surface was performed by the liquid phase designed dispersion method. A calculated amount of $Ti-VO(acac)_2$ was dissolved in 100 mL of zeolite dried toluene. The dried SBA-15 was added, and the solution was stirred for 1 h. After reaction, the modified support was filtered off, washed few times with toluene and dried under vacuum. The reaction was carried out at room temperature and in absence of air. The adsorbed complex is called the precursor. The acac ligands were removed by calcination, which was performed in a programmable oven at 550 °C in air. Two different paths to achieve the final TiO_x-VO_x mixed oxide catalyst were followed:

(a) The first involves sample **1** in which V−acac was deposited on Ti−acac/SBA-15 precursor: A calculated amount of $TiO(acac)_2$ was deposited on the SBA-15 by MDD. The precursor obtained was outgassed under vacuum conditions overnight. An estimated amount of $VO(acac)_2$ was then deposited on Ti−acac/SBA-15 surface, also by liquid phase. The sample obtained was filtered, washed off, dried under vacuum, and calcined at 550 °C to create the supported titanium−vanadium mixed oxide. Deposition was carried out at room temperature. For both depositions, the calculated concentrations of $TiO(acac)_2$ and $VO(acac)_2$ are the same.

(b) The second involves sample **2** in which V−acac was deposited on TiO_x/SBA-15 calcined: A calculated amount of $TiO(acac)_2$ was deposited on the SBA-15 by MDD. The precursor obtained was calcined at 550 °C. After that, an estimated amount of $VO(acac)_2$ was deposited on the TiO_x-SBA-15 support, which was filtered, washed off, dried in a vacuum, and calcined at 550 °C. Deposition was carried out at room temperature.

TABLE 2: Structural Parameters and Final Metal Loading of the Precursor and Calcined Samples, Prepared by the MDD Method

	final loading		structural properties			
	mmol V	mmol Ti	S_{BET} (m^2/g)	mesopore vol (cm^3/g)	micropore vol (cm^3/g)	total pore vol (cm^3/g)
1	0.12	0.52	401	0.40	0.02	0.42
1, calcined	0.12	0.52	525	0.50	0.05	0.55
2	0.25	0.55	372	0.44	0.03	0.47
2, calcined	0.25	0.55	492	0.49	0.07	0.56
3	0.2		43	0.08	0	0.08
3, calcined	0.2		143	0.21	0	0.21
4	0.2		453	0.48	0.05	0.53
4, calcined	0.2		596	0.52	0.10	0.62

The synthesis parameters were optimized in order to obtain the final mixed-oxide catalysts.[15] Mixed-oxide depositions were carried out calculating the concentration of Ti needed to react with 50% of the OH of the SBA-15 and calculating the concentration of V to react with the other 50% of the OH remaining on the SBA-15 surface.

The denotation and the final metal loading of samples **1**−**4**, prepared by the MDD method, are summarized in Table 2.

Methods. The concentration of the metals on the support was determined by *ultraviolet and visible (UV−Vis) spectrophotometry* after destruction of the samples and measured colorimetrically. The measurements were performed on a Unicam 8700 UV−Vis. For the single deposition, the samples were stirred for 20 min in hot sulfuric acid (2.5 M). After filtration, H_2O_2 was added, and vanadium concentration was measured at 450 nm. For the mixed oxide deposition, the signals of both complexes are too close and they interfere. HF prevents the formation of a color-Ti^{4+} complex; therefore, the concentrations of both metals can be analyzed separately, in the same way as in the single deposition.[16]

Porosity and surface-area studies were performed on a Quantachrome Autosorb 1 MP instrument. N_2 adsorption−desorption isotherms were recorded at 77 K. The Brunauer−Emmett−Teller (BET) model was used to calculate the specific surface area. The pore diameter was calculated using the Barret−Joyner−Halenda (BJH) method.[17] The micropore volume was calculated by the *t*-plot analysis, and the total pore volume was calculated by means of the total amount of adsorbed gas at $P/P_0 = 0.98$. The samples were outgassed overnight at room temperature for the precursors or at 200 °C for the supported oxides.

Fourier Transform infrared photoacoustic spectra (FTIR−PAS) were recorded on a Nicolet 20 SX spectrometer, equipped with a McClelland photoacoustic cell, to ensure IR measurements under dry conditions. About 500 scans were taken with a resolution of 8 cm^{-1}. The PAS spectrometer was placed in an isolated bench, which was constantly purged with nitrogen to ensure that the samples were completely dried.

The *continuous-wave (CW) EPR spectra* were recorded on a Bruker ESP300E spectrometer (microwave frequency 9.43 GHz) equipped with a gas-flow cryogenic system, allowing operation from room temperature down to 2.5 K. All presented spectra were recorded with a microwave power of 10 mW, a modulation frequency of 100 kHz, and a modulation amplitude of 0.5 mT. The magnetic field was measured using a Bruker ER 035 M NMR gaussmeter. The CW-EPR spectra were simulated using the EasySpin program (www.esr.ethz.ch).

All *pulse-EPR spectra* were recorded on a Bruker ESP380E spectrometer (microwave frequency 9.77 GHz) equipped with

a liquid Helium cryostat from Oxford Inc. The spectra were taken at 4 K, with a repetition rate of 1 kHz.

Electron-spin−echo (ESE)-detected EPR: The experiments were carried out with the pulse sequence $\pi/2-\pi-\tau-$echo, with pulse lengths $t_{\pi/2} = 16$ ns and $t_\pi = 32$ ns, and a τ value of 200 ns.

Two-Pulse Electron Spin−Echo Envelope Modulation (ESEEM) Experiments.[18] The experiments were carried out with the pulse sequence $\pi/2-\tau-\pi-\tau-$echo, with pulse lengths $t_{\pi/2} = 16$ ns and $t_\pi = 32$ ns, and the τ value was varied in steps of 8 ns. The two-pulse ESEEM spectra were used to determine the phase-memory time T_m.

Three-Pulse ESEEM Experiments.[18] The experiments were carried out with the pulse sequence $\pi/2-\tau-\pi/2-T-\pi/2-\tau-$echo with pulse lengths $t_{\pi/2} = 16$ ns and $t_\pi = 16$ ns. The time interval T was varied from 96 to 4184 ns in steps of 8 ns. The time interval τ was varied in steps of 16 ns from 96 to 320 ns. A four-step phase cycle was used to eliminate unwanted echoes. The time traces of the three-pulse ESEEM spectra were baseline-corrected in the T dimension with a third-order polynomial, apodized with a Hamming window, and zero filled. After a one-dimensional Fourier transformation (in the T dimension), the absolute value spectra were calculated. The spectra were added for the different τ values in order to eliminate blind-spot effects.

HYSCORE (Hyperfine Sublevel Correlation).[19] The experiments were carried out with the pulse sequence $\pi/2-\tau-\pi/2-t_1-\pi-t_2-\pi/2-\tau-$echo with pulse lengths $t_{\pi/2} = 16$ ns and $t_\pi = 16$ ns. The time intervals t_1 and t_2 were varied from 96 to 3288 ns in steps of 8 ns. A value of 96 ns was taken for τ. An eight-step phase cycle was used to eliminate unwanted echoes. The time traces of the HYSCORE spectra were baseline-corrected with a third-order polynomial, apodized with a Hamming window and zero filled. After two-dimensional Fourier transformation, the absolute value spectra were calculated.

Combination-peak Experiment.[18] The experiments were carried out with the pulse sequence $\pi/2-\tau-\pi/2-T-\pi-T-\pi/2-\tau-$echo with pulse lengths $t_{\pi/2} = 16$ ns and $t_\pi = 16$ ns. The time intervals T were varied from 96 to 3288 ns in steps of 8 ns. Different τ values were taken to eliminate the blind spots. An eight-step phase cycle was used to eliminate unwanted echoes. The time traces of the combination-peak spectra were baseline-corrected in the T dimension with a third-order polynomial, apodized with a Hamming window and zero filled. After one-dimensional Fourier transformation, the absolute value spectra were calculated. The spectra were added for the different τ values in order to eliminate blind-spot effects.

Results

1. CW-EPR Experiments. Figures 1 and 2 show the CW EPR spectra of **1** (1a), **2** (1b), **3** (2a), **4a** (2b), **4b** (2c), and **5** (2e) at room temperature. The EPR spectra of **1** and **2** show the characteristics of VO^{2+} complexes with vanadium in square-pyramidal coordination. They differ only slightly in their principal g and ^{51}V hyperfine values (Table 3). Upon lowering of the temperature, only an increase in intensity but no change in the spectral features was observed (not shown). This indicates that the vanadyl complexes are immobilized on the support. The CW-EPR spectra of the samples measured directly after synthesis (dry) or after substantial exposure (several weeks) to air (wet) showed no marked difference in the spectral form.

The CW-EPR spectrum of **3** at room temperature (Figure 2a) shows a similar axial spectrum as found for **1** and **2**. This EPR signal overlaps with a broad signal around $g \approx 1.98$, which is usually assigned to a high local spin concentration of vanadyl complexes, whereby the signal is dipolar broadened.[20−23] This indicates that the dispersion of the $VO(acac)_2$ complexes on the TiO_2 support is less efficient than that in **1** and **2**. Note however that the broadening may also be nonrelaxational in nature[21] (see further, pulse EPR measurements). The EPR parameters of **3** are markedly different from those of **1** and **2**, indicating a clear difference in the local environment (Table 3) and showing that the VO^{2+} complexes in **1** are not sensing a predominant TiO_x environment.

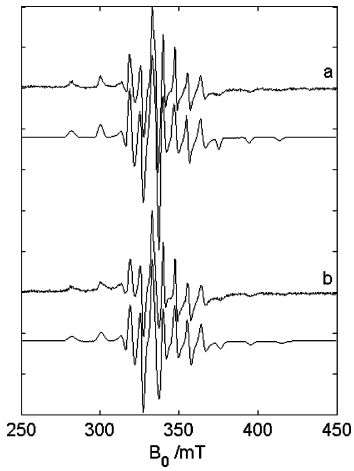

Figure 1. Experimental (top) and simulated (bottom) CW-EPR spectra at 298 K of (a) **1** ($VO(acac)_2/TiO(acac)_2$/SBA-15) and (b) **2** ($VO(acac)_2/TiO_x$/SBA-15). The microwave frequency was 9.43 GHz.

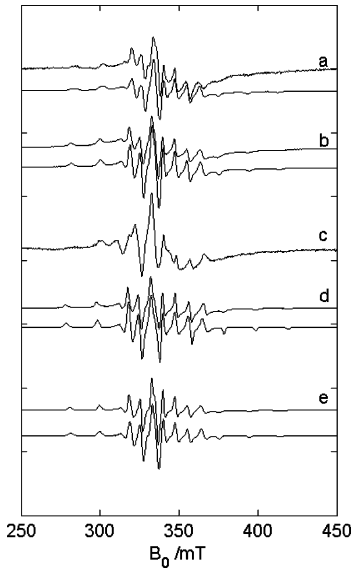

Figure 2. Experimental (top) and simulated (bottom) CW-EPR spectra of (a) **3** ($VO(acac)_2/TiO_x$) at 298 K, (b) **4a** ($VO(acac)_2$/SBA-15 (dry)) at 298 K, (c) **4b** ($VO(acac)_2$/SBA-15 (wet)) at 298 K, (d) **4b** at 20 K, and (e) **5** ($VO(acac)_2/TiO(acac)_2$) at 298 K. The microwave frequency was 9.43 GHz.

TABLE 3: Principal g and ^{51}V Hyperfine Values for the Samples under Study

samples	A_z/MHz (±2)	$A_{x,y}$/MHz (±3)	g_z (±0.001)	$g_{x,y}$ (±0.002)
1	511	191	1.936	1.976
2	514	193	1.932	1.975
3	495	181	1.934	1.973
4a	510	190	1.937	1.977
4b	543	200	1.930	1.976
5	515	193	1.937	1.975
6	518	193, 176	1.942	1.978, 1.982
7	513	191, 166	1.946	1.975, 1.980

Figure 2b shows the CW-EPR spectrum of $VO(acac)_2$ on the SBA-15 support directly after synthesis (**4a**, dry). Similar to **3**, the EPR spectrum consists of an axial contribution and a broad signal. The EPR parameters of the former fraction are (within experimental errors) identical to the ones of **1** and **2** (Table 3). This suggests that the vanadyl complexes in **1** and **2** sense the silica surrounding. Lowering of the temperature had no effect on the EPR parameters of **4a** (not shown).

The EPR spectrum of **4** is found to change after weeks of exposure to (moist) air (**4b**) (Figure 2c). The EPR spectrum of **4b** also changes clearly upon lowering the temperature to 20 K (Figure 2d). At room temperature the axial spectrum shows some motional averaging (total spectral width decreases) compared to the low-temperature spectrum. This indicates a mobility of the VO^{2+} complexes at room temperature.[20,21] Since the motional averaging is not total (we do not observe an isotropic eight-line spectrum), the mobility of the VO^{2+} complexes on the SBA-15 is limited, which indicates still some interaction with the framework. The EPR parameters of the axial spectrum of **4b** at low temperatures (Table 3) are clearly different from the ones found for **4a**. In fact, they are very near to those reported for $VO(H_2O)_5^{2+}$ ($g_{x,y} = 1.978$, $g_z = 1.933$, $A_{x,y} = 212$ MHz, $A_z = 547$ MHz)[24] and for hydrated VO^{2+}-exchanged zeolites.[25] This indicates that, upon hydration of the sample, the VO^{2+} ions lose their acac ligands, which are replaced by water.

Figure 2e shows the EPR spectrum of 0.1 wt % $VO(acac)_2$ in 99.9 wt % $TiO(acac)_2$ (**5**) after exposure to air. The EPR parameters of the axial spectrum (Table 3) are similar to those observed for the axial contributions in **1**, **2**, and **4a**.

As a comparison, the EPR parameters of frozen toluene and ethanol solutions of $VO(acac)_2$ (**6** and **7**, spectra not shown) are given in Table 3. In toluene, the V^{4+} center is essentially pentacoordinated, whereas in ethanol a solvent molecule is coordinating axially as a sixth ligand.[26−28] This causes a change of color from blue-greenish to yellow-greenish. It should be noted that for **1**, **2**, **4a**, and **5** the A_z value is very near to the one observed for $VO(acac)_2$ in ethanol (**7**). Furthermore, the samples **1**, **2**, **4a**, and **5** have a yellow-greenish color. This may suggest interactions with hydroxyl groups of the support and/or water molecules.

Finally, the effect of heating samples **1** and **2** for 24 h at 100 °C was tested. This drying process caused a dramatic decrease of the CW-EPR intensity owing to V(IV) to V(V) conversion. The overall shape of the remaining spectrum was identical as that observed for the unheated samples.

2. ESE-Detected EPR Experiments and Phase-Memory-Time Determinations. To investigate further the possible differences in structure of **1** and **2**, pulsed EPR measurements were undertaken. Figure 3 shows the ESE-detected EPR spectra of the different samples. As references the ESE-detected EPR spectra of **6** and **7** were taken which gave a very intense Hahn echo. The spectrum of **7** is shown in Figure 3a and, as expected, the shape resembles in its first-derivative form closely the CW-EPR spectrum.

For sample **2** again an intense Hahn echo was observed and the corresponding ESE-detected EPR spectrum (Figure 3b) is analogous to the integrated form of the CW EPR spectrum. Comparison between parts a and b of Figure 3 reveals a far larger line width in the latter case. For **2**, the two-pulse echo signal at magnetic field setting $B_0 = 347.1$ mT was found to decay monoexponentially with a short phase-memory time, $T_m = 430$ ns. Analogous relaxation times were found at other magnetic field settings.

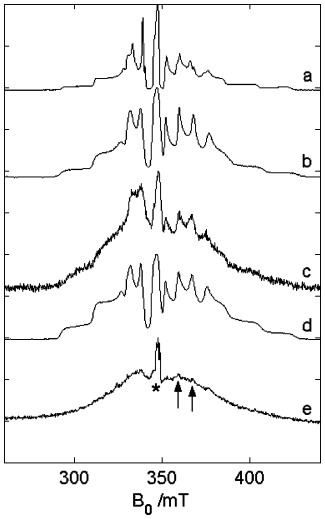

Figure 3. Experimental ESE-detected EPR spectra at 4 K of (a) **7** ($VO(acac)_2$ in ethanol), (b) **2** ($VO(acac)_2/TiO_x$/SBA-15), (c) **3** ($VO(acac)_2/TiO_x$), (d) **5** ($VO(acac)_2/TiO(acac)_2$), and (e) **1** ($VO(acac)_2/TiO(acac)_2$/SBA-15). The microwave frequency was 9.767 GHz. The experimental pulse EPR settings are mentioned in the text.

The Hahn echo of sample **3** was about a factor of 10 smaller than the one of sample **2**, which agrees with the difference in the CW-EPR intensity and which can be related to the smaller surface of TiO_2 vs SBA-15 (see Table 2). The corresponding ESE-detected EPR spectrum (Figure 3c) is similar to the CW-EPR spectrum (an axial spectrum with an underlying broad line). The axial component was again characterized by a short phase-memory time ($T_m = 350$ ns for $B_0 = 347.1$ mT). The underlying broad signal has a surprisingly long T_m of 2.2 μs. This shows that the line-broadening is not relaxational in nature (dipolar coupling) and does not stem from a high local spin concentration of vanadyl complexes.

The ESE-EPR spectrum of **5** is comparable to that of **2** with larger line widths than observed for **7** (compare Figure 2d with Figure 2a,b). The phase-memory time is again short ($T_m = 360$ ns for $B_0 = 346.8$ mT) and comparable to the ones found for the axial contributions found in the spectra of **2** and **3**.

For samples **4a** and **4b**, only a weak Hahn echo could be observed (>50 times lower than for **2**) and the corresponding magnetic field sweep learned that the majority of the ESE-detected EPR spectrum (not shown) was due to the cavity background signal (i.e., a copper-type signal in the 280−350 mT region), as could be determined from blank measurements. The correct positioning of the sample in the cavity was checked by measuring the CW-EPR spectrum prior to the pulse-EPR experiment. The inability to detect a component from the vanadyl species in these compounds at the interpulse times τ used, indicates that the phase-memory time T_m of these species is shorter than for the samples **2** and **3**. The fact that no broad signals could be detected in the ESE-detected EPR spectra, despite their occurrence in the CW-EPR spectra, proves that high local concentrations of vanadyl complexes are present and the broad signal results from dipolar broadening. The dispersion of the $VO(acac)_2$ molecules on the pure SBA-15 is thus not as good as in **2**, **3**, and **5**. This is in agreement with earlier observations that the dispersion of V improves considerably when first coating the surface of silica with TiO_2.[13,14]

Finally, for sample **1** a Hahn echo of a factor of 9 lower than for **2** was found (difference in CW-EPR intensity less than a factor of 2). The corresponding ESE-detected EPR spectrum (Figure 3e) is surprising. It shows a feature that is dominated

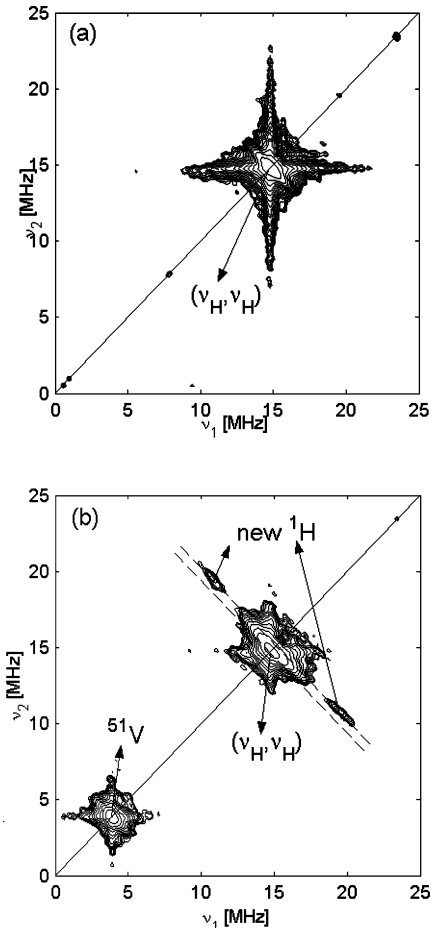

Figure 4. HYSCORE spectra with $\tau = 96$ ns taken at observer position 347.1 mT for (a) **6** ($VO(acac)_2$ in toluene) and (b) **2** ($VO(acac)_2/TiO_x$/SBA-15). The experimental pulse EPR settings are mentioned in the text.

by the broad line around $g = 1.98$. Furthermore, only a weak contribution of the axial component is found (see for instance the small signals at 359 and 367 mT (arrows in spectrum) corresponding to features in Figure 3a−d). This means that the phase-memory time T_m for this contribution is short ($T_m < 200$ ns). The fact that the axial contribution is almost completely missing from the ESE-detected spectrum explains the low Hahn-echo intensity, since the CW-EPR spectra showed that the resolved axial component is the dominant contribution for both **1** and **2** (Figure 1). The ESE-detected EPR spectrum shows also sharp lines in the 344 to 351 mT region at $g = 2.0135$, 2.0085, and 2.0031. These values are close to earlier reported g values for $O_2^- - V^{5+}$ species.[23] The observation of the broad signal is interesting. This signal was not resolved in CW-EPR spectra, where it is totally masked by the dominant axial contribution. The relatively long phase-memory time ($T_m = 2.8$ μs) proves that the signal does not stem from high local spin concentrations. The nature of the signal will be treated in the discussion.

3. ESEEM Experiments. To investigate further the local structure of the different $VO(acac)_2$ containing samples, ESEEM experiments were undertaken. Figure 4 shows the HYSCORE spectra of **6** and **2** respectively, taken at the magnetic-field setting 347.1 mT. At this field setting almost all orientations are excited, so that the spectrum reflects a powder-like situation. In the Supporting Information, the corresponding spectra of **5** and **7** are shown. In the HYSCORE spectrum of **6** we observe a ridge around the (ν_H, ν_H) (ν_H = proton Zeeman frequency) (Figure 4a). The contour lines in Figure 4a are deliberately set very low (hence the appearance of the star pattern of the tails of the central line) to ensure the reader that no proton coupling was missed. The edge of the ridge is at about (13.22, 16.44 MHz) indicating a maximum proton interaction of 3.22 MHz (±0.3 MHz). This agrees with the earlier ENDOR (electron nuclear double resonance) observation that the maximal proton hyperfine interaction for $VO(acac)_2$ in toluene is 3.35 MHz.[27] Analogous results with a slightly higher maximal splitting of 4.2 MHz were found for **7** (see Supporting Information). The increase in the maximal proton hyperfine interaction from **6** to **7** agrees with the axial coordination of ethanol to $VO(acac)_2$.

The HYSCORE spectrum of **2** shows peaks resulting from interactions with ^{1}H and with ^{51}V nuclei (Figure 4b). Note that the latter peak is not caused by the central ion hyperfine interaction, which is already observed in the EPR spectra, but by the interaction with the V nuclei of neighboring complexes. Most likely the signal stems from diamagnetic V(V) species as observed earlier for VO^{2+} complexes (VO^{2+} species are usually unstable in an oxygen-rich environment[29]). This is corroborated by the comparison with the results for **5** (Supporting Information). Indeed, as shown above, the phase-memory times T_m of **2** and **5** are in the same order, indicating that the local concentrations of paramagnetic species are approximately the same. However, the HYSCORE spectrum of **5** has no marked peak at (ν_V,ν_V) (see Supporting Information). The ^{51}V ridge observed in the HYSORE spectrum of **2** must thus arise from ^{51}V nuclei in diamagnetic molecules. The ^{51}V ridge has a maximum width of 2.8 MHz (lowest contour lines). In the case this splitting arises from a pure dipolar coupling whereby the nuclear-quadrupole is assumed to be quasi-zero, this value is equal to $2T$ with

$$T = (\mu_0/4\pi) g_e g_n \beta_e \beta_n / h^3 \qquad (1)$$

with r the distance between the unpaired electron and the ^{51}V nucleus. This puts a lower limit for the distance of 0.25 nm between the central VO^{2+} and the adjacent ^{51}V can be deduced. Note, however, that the nuclear-quadrupole coupling will not be zero and that this value is thus underestimated. Furthermore, the analysis of the three-pulse ESEEM modulation at the ^{51}V Lamor frequency (not shown) puts an upper limit to this distance of 0.85 nm. It should again be noted that the unknown nuclear-quadrupole coupling of the ^{51}V nucleus can have a large effect on the ESEEM modulation depth, making an accurate distance determination using this method impossible.[30] Furthermore, a distribution in the distances is expected.

Although the echo signal of $VO(acac)_2$ on the TiO_2 support (**3**) was too low to obtain a sufficient signal/noise ratio for the HYSCORE experiments, three-pulse ESEEM experiments could be performed (Figure 5). These show that the ^{51}V signal is also present in sample **3**. We observe a difference in the ratio of the intensities of the peaks at ν_V and ν_H between **2** and **3**, whereby the H/V ratio in the direct environment of the vanadyl centers seems to be higher for **2** than for **3**.

In the HYSCORE spectra of **2** and **5** we see ridges belonging to a ^{1}H interaction not observed in **6** and **7** (signals marked "new ^{1}H" in Figure 4b; Supporting Information). The maximum splitting is now 11.02 MHz. To determine the anisotropy of the hyperfine interaction, combination-peak experiments[18] were undertaken for **2** in comparison with **6** and **7** (Figure 6). In the combination-peak experiments, the maximal shift Δ_{max} of the proton sum peak from twice the proton Zeeman frequency, $2\nu_H$,

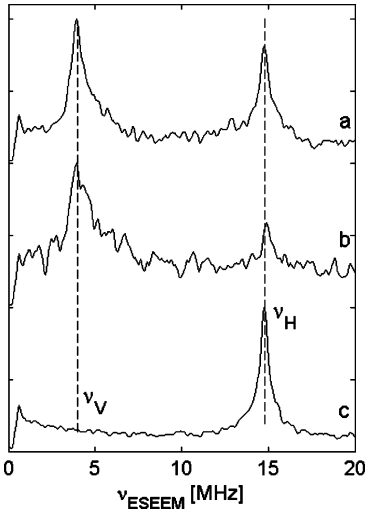

Figure 5. Three-pulse ESEEM spectra at observer position 347.1 mT for (a) **2** ($VO(acac)_2/TiO_x$/SBA-15), (b) **3** ($VO(acac)_2/TiO_2$), and (c) **6** ($VO(acac)_2$ in toluene). The experimental pulse EPR settings are mentioned in the text.

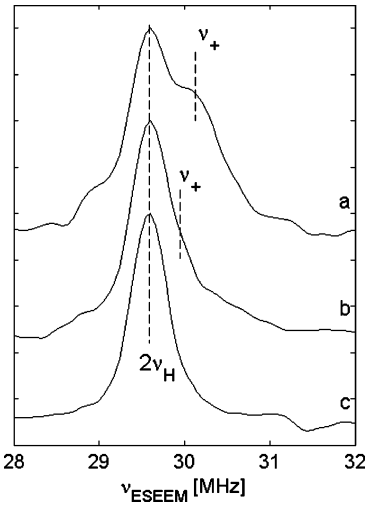

Figure 6. Combination-peak spectra taken at observer position 347.1 mT for (a) **2** ($VO(acac)_2/TiO_x$/SBA-15), (b) **7** ($VO(acac)_2$ in ethanol), and (c) **6** ($VO(acac)_2$ in toluene). The experimental pulse EPR settings are mentioned in the text

depends on the dipolar coupling T [31]

$$\Delta_{max} \approx 9T^2/16\nu_H \qquad (2)$$

with T given in eq 1 and r now the distance between the proton and the unpaired electron.

For **6**, we find that the proton combination-peak appears at $2\nu_H$ and that essentially no shift vs this position is observed. This agrees with the hyperfine couplings from earlier ENDOR data on $VO(acac)_2$ in toluene, from which maximal shifts of only 0.11 MHz are expected. For **7** we find a bigger maximal shift ($\Delta_{max} = \nu_+ - 2\nu_H$ in Figure 6) of 0.38 MHz (±0.1). According to eqs 1 and 2 this agrees with $T = 3.15$ MHz (±0.3) and $r = 0.29$ (±0.01) nm. Comparison with ENDOR studies of VO^{2+} and $VO(acac)_2$ complexes in alcoholic solvents[26,32] shows that these parameters agree with the ones found for the hydroxyl proton of the axially coordinating solvent molecule. It is clear from Figure 6a, that the maximal shift of the sum peak is much larger in the case of **2** ($\Delta_{max} = 0.59$ MHz (±0.1)). This corresponds to $T = 3.95$ (±0.3) MHz and $r = 0.270$ (±0.005) nm. These parameters agree well with the ones found for equatorial OH coordination to the VO^{2+}.[32] Also the maximal proton splitting (11.02 MHz) is in accordance with what is observed for the equatorial OH of VO^{2+} in methanol.[32] This indicates that the $VO(acac)_2$ complex is no longer in its original coordination. Analogous observations were made for **5** (see Supporting Information).

4. FTIR−PAS Spectroscopy. Figure 7 shows the infrared study of the metal acetylacetonate modified SBA-15 support (**4**), exhibiting the characteristic acac vibrations in the region 1700−1300 cm^{-1}.

Figure 7a presents the IR spectrum of the acac vibrations of the $VO(acac)_2$ on SBA-15 (sample **4**) over time. After exposure to air for 3 days, the sample has lost almost completely its acac ligands (Figure 7a-iii). This is in agreement with the EPR studies, which show a significant difference between a dry sample and a wet sample after being exposed to air (Figure 2c,d). This agrees with the fact that $VO(acac)_2$ complexes tend to increase their coordination sphere by coordinating water molecules in the 6-fold position that is still available. Then, it is the water molecule that promotes the easy release of the acac ligands by proton-assisted hydrolysis to form acetylacetonate, which is lost from the complex.[33]

This tendency is less pronounced in the case of $TiO(acac)_2$ complexes or when $VO(acac)_2$ is present in a $TiO(acac)_2$ environment as becomes evident from the following. In Figure 7b the IR−PAS spectra of a dry $TiO(acac)_2$ on SBA-15 (i), of the same sample after few hours outside of the glovebox in air (ii) and of the wet sample (iii) are shown. The spectrum in Figure 7b-iii shows almost no decrease of the acac bands after a long air exposure. In contrast to the $VO(acac)_2$ complex, titanyl acetylacetonate is a bidentate complex ($[TiO(acac)_2]_2$), which consists of a cyclic dimer with the Ti atoms linked through oxygen atoms.[34] In this case, the Ti complex has a 6-coordination so it is unlikely to coordinate with water and to lose an acac ligand as in the case of $VO(acac)_2$. Besides that, $TiO(acac)_2$ is bulkier and therefore water molecules are sterically hindered from approaching the complex.

The CW-EPR results did not show a large difference between the dry and wet form of the mixed-oxide precursors **1** and **2**. This is again confirmed by the IR−PAS results (Figure 7c,d), in which the intensity of the acac region for both samples decreases only very little during air exposure in contrast to the pronounced change observed for **4**. This is due to the presence of the $TiO(acac)_2$ complexes that are either formed during synthesis (in precursor sample **1**), or that are formed after migration of the acac ligands from V to Ti-centers (in the case of sample **2**), as was proven earlier.[15] Because of the presence of the bulky Ti−acac and the covalent interaction between V and Ti, the full replacement of the acac ligands of the vanadyl complexes with water is less likely to occur.

5. Characterization of the TiO_x—VO_x Mixed Oxides: Porosity Analysis. The calculated structural parameters, such as specific surface area, S_{BET}, BJH pore radius, and mesopore and micropore volume, are summarized in Table 2 for the different precursor and calcined samples.

The calculated BET surface area for the calcined SBA-15 support material is between 600 and 800 m^2/g, while this value decreases with increasing metal loading. The pores of the SBA-15 support are filled by grafting the surface OH groups with the metal acac complexes. As a result, the porosity and surface area are reduced. They increase again after calcination of the precursor, as the metal complexes are converted into the V−Ti mixed oxides.

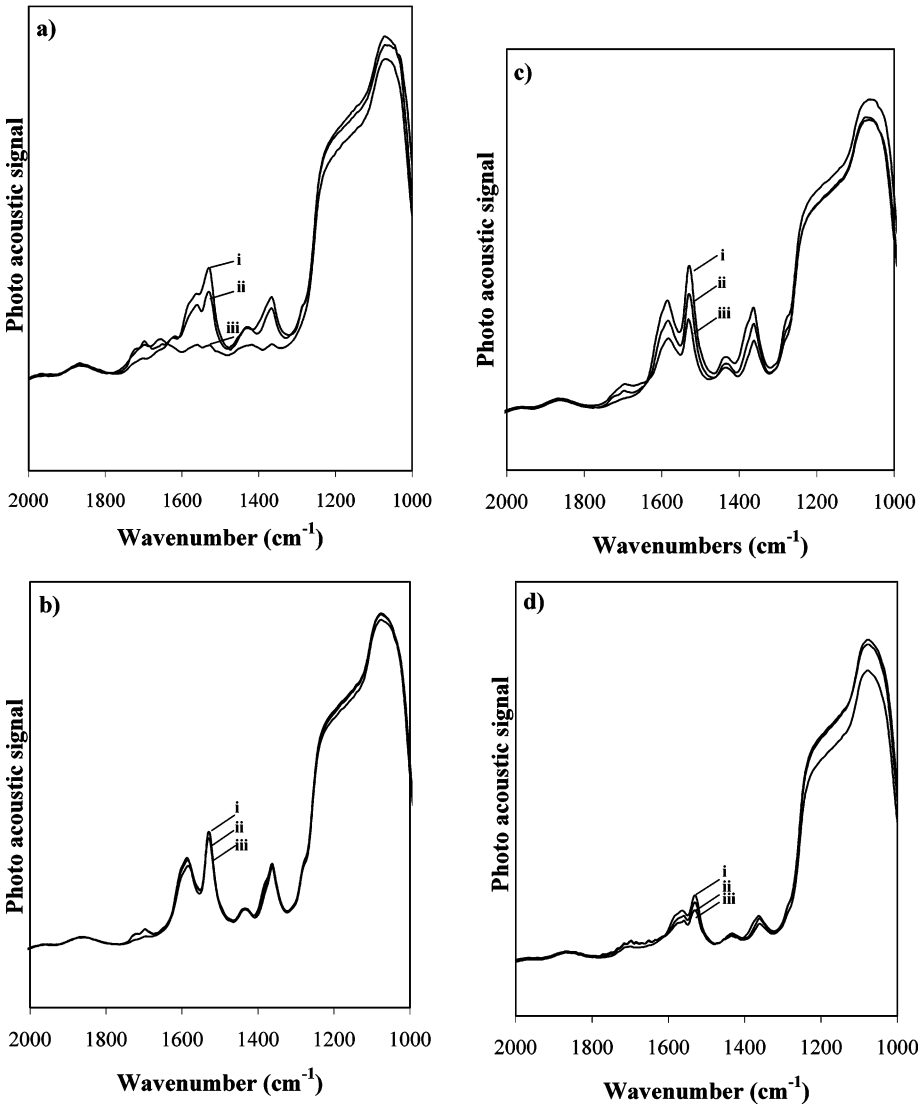

Figure 7. FTIR−PAS spectra of the acac vibrations of (a) precursor $VO(acac)_2$ on SBA-15 (**4**), (b) $TiO(acac)_2$ on SBA-15, (c) mixed oxide $VO(acac)_2/TiO(acac)_2$−SBA15 (**1**), and (d) mixed oxide $VO(acac)_2/TiO_x$-SBA15 (**2**) measured as (i) dry sample, (ii) sample after a short air exposure (few hours) and (iii) sample after 3 days air exposure.

Our earlier measurements of the nitrogen adsorption/desorption isotherms[15] of pure SBA-15 and **1** and **2** in their precursor and calcined form, indicated that samples **1** and **2** differ in pore structure, as a result of the different way of preparation (see also Supporting Information).

In sample **2**, the Ti−acac complex is first calcined and spread out along the hexagonal channels of the SBA-15 material. Then, after calcination, V−acac is deposited. In this way, the vanadium centers are able to react with the OH of the SBA-15 as well as with TiO_x, and as a result the double amount of V can be deposited compared to sample **1** (Table 2). Upon calcination, vanadium is spread out, mainly, over the titanium layer inside the channels of the support. This leads to an open mesopore structure for the SBA-15 catalyst, as proven by N_2 adsorption−desorption.[15] However, after calcinations of **1** plugs of metal oxides are found (see Supporting Information). The structure is a combination of open and blocked cylindrical mesopores. In this case, the Ti−acac complexes are deposited first, not calcined, and bulky V−acac complexes are immediately deposited afterward. In this way, bulky Ti−acac complexes block the entrances of the pores. The V−acac will only react with the OH of the SBA-15, remaining at the pore entrances, forming the plugs after calcination.

Discussion

The CW-EPR spectra of **1** and **2** are dominated by an axial contribution, typical for vanadium in a square-pyramidal coordination. The EPR parameters are quasi-identical for both samples and are close to the ones of the axial contribution in the spectra of **4a** and **5**. They differ, however, strongly from the axial component in **3**. This indicates that in **1** and **2** the $VO(acac)_2$ molecules are not embedded in a pure titanium−oxide environment but that SBA-15 must still be interacting with the $VO(acac)_2$ complex.

From Table 3 and from the literature[26,27] it becomes clear that an axial solvent coordination to the $VO(acac)_2$ causes a slight lowering of the A_z value. It should be noted that for **1**, **2**, **4a**, and **5** the A_z value is very near to the one observed for $VO(acac)_2$ in ethanol (**7**). Furthermore, the samples **1**, **2**, **4a**, and **5** have a yellow-greenish color. This may suggest interactions with hydroxyl groups of the support and/or water molecules.

Both the CW-EPR and IR spectra show that for $VO(acac)_2$ on SBA-15 (**4**) exposure to air causes a rapid loss of the acac ligands and replacement by water. Upon longer exposure of **1** and **2** to air, the CW-EPR spectra are not changing significantly (except for a decrease in intensity due to V(IV) to V(V)

conversion). Accordingly, the IR spectra show a much smaller replacement of the acac ligands in **1** and **2** by water than observed for $VO(acac)_2$ on SBA-15 (Figure 7).

Furthermore, the CW-EPR spectra of **4a** and **4b** reveal a large contribution of a broad signal at $g = 1.98$. The ESE-detected EPR experiments prove that this signal stems from high local concentration of $VO(acac)_2$ complexes, proving a poor dispersion of the complexes on the pure SBA-15 support. Samples **1** and **2** are lacking this contribution implying that the $VO(acac)_2$ complexes can better migrate in these cases.

The CW-EPR spectrum of **3** also shows a contribution of a broad signal, but the observed T_m value now proves that the line broadening cannot be ascribed to high local spin concentrations. Two possible explanations can be put forward. First, the broad feature may stem from a multitude of isolated VO^{2+} complexes with different ligation and/or surrounding and consequent different EPR parameters. The summation of all individual spectra will lead to broad signal with the spectral width typical for vanadyl species but without clearly resolved peaks. Indeed, T_m values of several microseconds have been reported for diluted vanadyl complexes.[35] On the other hand, broad signals with substantial T_m have been detected in crystalline vanadium pentoxide.[21] These signals have been attributed to localized d-electrons interacting with between two and four ^{51}V nuclei giving rise to a poor resolution in the EPR spectra. Since partial oxidation from V(IV) to V(V) in air is likely to happen, the observed signal may arise from microcrystalline V_2O_5 on the titanium oxide support. This may agree with the relatively higher three-pulse ESEEM signal at ν_V than at ν_H compared to the **2** (Figure 5) indicating a relatively higher V/H ratio.

An analogous broad contribution is observed in the ESE-detected EPR spectra of **1**, indicating a heterogeneity, which was not detected with CW-EPR spectroscopy. Since the two-pulse echo decay of **2** is monoexponential, lacking the slower relaxation related to the broad signal in **1**, this seems to indicate that the synthesis pathway of **2** leads to a more defined local structure of the VO^{2+} complexes than in **1**. Furthermore, the T_m value of the sharp axial component in **1** is smaller than in **2**. Since the T_m value decreases with increasing spin concentration, this indicates that the vanadyl complexes in **1** are closer to each other than in **2**. This can be related to the partial blocking of the pores by the bulky $TiO(acac)_2$ complex in **1**, making the dispersion less efficient. This was evidenced earlier when the structural changes of the different samples were investigated[15] (see also porosity-analysis section). The dispersion of $VO(acac)_2$ increases following the scheme **2** > **1** > **4**.

From the IR measurements we have seen that, although the acac-ligand replacement in **1** and **2** is less than in **4** upon air exposure, there is some loss of acac ligands. This is corroborated by the HYSCORE spectra of **2**, showing that equatorial OH coordination has occurred. Several possibilities can be thought of. The $VO(acac)_2$ may have lost one of its acac ligands and taken up an equatorial ligand or may have changed from a cis to a trans form as was observed for other $VO(acac)_2$ complexes in the combination with coordinating solvent.[28,36] As to the nature of the coordinating molecule one might put forward H_2O (the sample was exposed to air) or hydroxyl groups on the TiO_2 or the silica surface, which are formed after the calcination process. Several indications point to an acac replacement by water. First, there is the observed increase in the water-related peak in the IR spectra in correlation with the decrease of the acac-related signals. Furthermore, analogous signals from equatorial protons were found in **5**, where no surface hydroxyl groups are present. The exchange of the acac ligands to water is however much smaller than for $VO(acac)_2$ on pure SBA-15 (**4**), for which exposure to air leads to a full replacement of the acac ligands and incrased motional liberties of the VO^{2+} complexes.

Conclusions

TiO_x-VO_x mixed oxides supported SBA-15 catalysts were prepared in a controlled way using two different synthetic pathways. The final catalysts show clear differences in the degree of blockage of the mesopores depending on the chosen synthesis route. Using CW and pulsed EPR spectroscopy, it is shown that these differences can already be traced back to the $VO(acac)_2$-containing precursors. Both the local concentration of the vanadyl complexes and the degree of heterogeneity is found to differ for the two precursors. Furthermore, it is shown that the fast, full exchange of the acac ligands to water, occurring in $VO(acac)_2$ on a pure SBA-15 support, is largely hampered in the presence of TiO_x or $TiO(acac)_2$ complexes and that the presence of the titanium allows for a better dispersion of the $VO(acac)_2$ complexes.

Acknowledgment. P.C. and S.V.D. acknowledge the FWO-Flanders (Fund for Scientific Research-Flanders) for financial support.

Supporting Information Available: Figures showing pulse-EPR spectra of **5** and **7** and nitrogen adsorption−desorption isotherms at 77 K of **1** and **2**. This material is available free of charge via the Internet at http://pubs.acs.org

References and Notes

(1) Mathieu, M.; Van der Voort, P.; Weckhuysen, B. M.; Rao, R.; Catana, G.; Schoonheydt, R. A.; Vansant, E. F. *J. Phys. Chem. B* **2001**, *105*, 3393−3399.

(2) Parvulescu, V. I.; Boghosian, S.; Parvulescu, V.; Jung, S. M.; Grange, P. *J. Catal.* **2003**, *217*, 172−185.

(3) Newalkar, B. L.; Olanrewaju, J.; Komarnei, S. *J. Phys. Chem. B* **2001**, *105*, 8356−8360.

(4) Lietti, L.; Alemany, J. L.; Forzatti, P.; Busca, G.; Ramis, G.; Giamello, E.; Bregani, F. *Catal. Today* **1996**, *29*, 143−148.

(5) Fornes, V.; Lopez, C.; Lopez, H. H.; Marinez, A. *Appl. Catal., A* **2003**, *249*, 345−354.

(6) Liu, Y.-M.; Cao, Y.; Zhu, K.-K.; Yan, S.-R.; Dai, W.-L.; He, H.-Y.; Fan, K.-N. *Chem. Commun.* **2002**, 2832−2833.

(7) Reiche, M. A.; Ortelli, E.; Baiker, A. *Appl. Catal., B* **1999**, *23*, 187−203.

(8) Finocchio, E.; Baldi, M.; Busca, G.; Pistarino, C.; Romezzano, G.; Bregani, F.; Toledo, G. P. *Catal. Today* **2000**, *59*, 261−268.

(9) Van der Voort, P.; White, M. G.; Vansant, E. F. *Langmuir* **1998**, *14*, 106−112.

(10) Baltes, M.; Collart, O.; Van der Voort, P.; Vansant, E. F. *Langmuir* **1999**, *15*, 5841−5845.

(11) Van der Voort, P.; van Welzenis, R.; de Ridder, M.; Brongersma, H. H.; Baltes, M.; Mathieu, M.; van de Ven, P. C.; Vansant, E. F. *Langmuir* **2002**, *18*, 4420−4425.

(12) Schrijnemakers, K.; Vansant, E. F. *J. Porous Mater.* **2001**, *8*, 83−90.

(13) Tesser, R.; Maradei, V.; Di Serio, M.; Santamaria, E. *Ind. Eng. Chem. Res.* **2004**, *43*, 1623−1633.

(14) Quaranta, N. E.; Cortes Corberan, V.; Fierro, J. L. G. *Stud. Surf. Sci. Catal.* **1992**, *72*, 147.

(15) Segura, Y.; Cool, P.; Van der Voort, P.; Mees, P.; Meynen, V.; Vansant, E. F. *J. Phys. Chem. B* **2004**, *108*, 3794−3800.

(16) Vogel, A. I. *Quantitative Inorganic Analysis*, 3rd ed.; Longman: London, 1971; p 790.

(17) Rouquerol, F., Rouquerol, J., Sing, K. *Adsorption by powders and porous solids*; Academic Press: San Diego, CA, 1999; p 191.

(18) Schweiger, A.; Jeschke, G. *Principles of pulse electron paramagnetic resonance*; Oxford University Press: Oxford, England, 2001.

(19) Höfer, P.; Grupp, A.; Nebenführ H.; Mehring, M. *Chem. Phys. Lett.* **1986**, *132*, 279−282.

(20) Luan, Z.; Kevan, L. *J. Phys. Chem.* **1997**, *101*, 2020−2027.

(21) Luca, V.; MacLachlan, D. J.; Bramley, R. *Phys. Chem. Chem. Phys.* **1999**, *1*, 2597−2606.
(22) Baltes, M.; Cassiers, K.; Van Der Voort, P.; Weckhuysen, B. M.; Schoonheydt, R. A.; Vasant, E. F. *J. Catal.* **2001**, *197*, 160−171.
(23) Quaranta, N. E.; Soria, J.; Cortes Corberan, V.; Fierro, J. L. G. *J. Catal.* **1997**, *171*, 1−13.
(24) Chasteen, N. D. In *Biological Magnetic Resonance*; Berliner, L.; J. Rueben, J., Eds.; Plenum: New York, 1981; Vol. 3, p 53.
(25) Carl, P. J.; Isley, S. L.; Larsen, S. C. *J. Phys. Chem. A* **2001**, *105*, 4563−4573.
(26) Kirste, B.; van Willigen, H. *J. Phys. Chem.* **1982**, *86*, 2743−2749.
(27) Yordanov, N. D.; Zdravkova, M. *Polyhedron* **1993**, *12*, 635−639.
(28) Amin, S. S.; Cryer, K.; Zhang, B.; Dutta, S. K.; Eaton, S. S.; Anderson, O. P.; Miller, S. M.; Reul, B. A.; Brichard, S. M.; Crans, D. C. *Inorg. Chem.* **2000**, *39*, 406−416.
(29) Pöppl, A.; Manikandan, P.; Köhler, K.; Maas, P.; Strauch, P.; Böttcher, R.; Goldfarb, D. *J. Am. Chem. Soc.* **2001**, *123*, 4577−4584.
(30) Luca, V.; MacLachlan, D. J.; Bramley, R. *Phys. Chem. Chem. Phys.* **1999**, *1*, 2597−2606.
(31) Reijerse, E. J.; Dikanov, S. A. *J. Chem. Phys.* **1991**, *95*, 836−845.
(32) Mustafi, D.; Makinen, M. W. *Inorg. Chem.* **1988**, *27*, 3360−3368.
(33) White, M. G. *Catal. Today* **1993**, *18*, 73−119.
(34) Smith, G. D.; Caughlan, C. N.; Campbell, J. A. *Inorg. Chem.* **1972**, *11*, 2989−2993.
(35) Du, J. L.; Eaton, G. R.; Eaton, S. S. *J. Magn. Reson. A* **1996**, *119*, 240−246.
(36) Murphy, D. M.; Fallis, I. A.; Farley, R. D.; Tucker, R. J.; Avery, K. L.; Willock, D. J. *Phys. Chem. Chem. Phys.* **2002**, *4*, 4937−4943.